metals

MDPI

Article

Investigation of the Heat Treatment Process and Formation Mechanism of Grain Boundary Serration for GH4795 Superalloy

Shuo Huang [1,2], Wenyun Zhang [1], Bingchao Xie [3], Hao Yu [3], Yongquan Ning [3,*] and Beijiang Zhang [1,*]

[1] High Temperature Materials Research Division, Central Iron & Steel Research Institute, Beijing 100081, China
[2] Pangang Group Panzhihua Research Institute of Iron and Steel Co., Ltd., Panzhihua 617000, China
[3] School of Materials Science and Engineering, Northwestern Polytechnical University, Xi'an 710072, China
* Correspondence: luckyning@nwpu.edu.cn (Y.N.); bjzhang@cisri.com.cn (B.Z.)

Abstract: Heat treatments, including solution treatment and isothermal heat treatment, were conducted to investigate the grain boundary serration of GH4975 superalloy. The two different heat treatment processes could both promote the formation of serrated grain boundaries within the present temperature and soaking time ranges, provided that the cooling rates were controlled to be quite slow. The samples subjected to furnace cooling exhibited a more obvious serrated grain boundary morphology by comparison with those subjected to air cooling. The interaction between precipitated phases and grain boundaries was focused to explore the formation mechanisms of serrated grain boundaries within GH4975 superalloy. Heat treatment temperature and soaking time strongly affected the morphology and size of precipitated phases, and consequently influenced the formation of serrated grain boundaries. The directional growth of grain boundary precipitates and its pinning effects on the migration of grain boundaries also affected the grain boundary morphology.

Keywords: Ni-based superalloy; heat treatment; serrated grain boundary; boundary precipitates; serration mechanism

Citation: Huang, S.; Zhang, W.; Xie, B.; Yu, H.; Ning, Y.; Zhang, B. Investigation of the Heat Treatment Process and Formation Mechanism of Grain Boundary Serration for GH4795 Superalloy. *Metals* **2022**, *12*, 1521. https://doi.org/10.3390/met12091521

Academic Editor: Chang Yong Jo

Received: 1 August 2022
Accepted: 13 September 2022
Published: 14 September 2022

1. Introduction

Ni-based superalloys have been widely used as turbine discs in aircraft engines due to their excellent properties, such as high-temperature mechanical properties, corrosion, and oxidation resistances [1–4]. However, the grain boundaries usually become weak at elevated temperatures, and hence it will be necessary to avoid the crack initiation on grain boundaries for better high-temperature performance [5–7]. Therefore, how to optimize the grain boundary morphology and its strength will be critical to improve the high-temperature properties of alloys [8,9]. Serrated grain boundaries were formed by the bending of straight grain boundaries under specific process conditions, such as isothermal treatments and controlled cooling heat treatments [10–12]. It has been proved that the presence of serrated grain boundary in Ni-based superalloy could enhance grain boundary effectively and improve their resistance to crack propagation [13–15].

Serrated grain boundary has importance industrial value for grain boundary engineering, which could impede grain boundary sliding and crack initiation [16,17]. Therefore, the serrated grain boundary formation mechanism needs to be investigated systematically. Many investigations have been conducted about the serrated grain boundary formation mechanism in Ni-based superalloy, mainly focused on the interaction between precipitating phases (such as γ' phase and grain boundary carbides) and grain boundaries [18–20]. Some researchers proposed that the formation of serrated grain boundary was closely related to the orientation of γ' phase on grain boundaries. Meanwhile, the morphology, size, and content of γ' phase also affected the bending of grain boundary [19,21]. Yang et al. [22] suggested that the grain boundaries began to serrate with the decrease of cooling rate

during the solution heat treatment in GH4710 alloy. The γ′ phase hindered the movement of grain boundaries in this process. Grain boundary serration has also been studied as a function of cooling rate in Ni-based superalloy. Based on the movement of grain boundary γ′ phase, a model for the displacement of local grain boundaries and the initiating of serrated grain boundary formation was proposed by Koul and Gessinger [16]. The net strain energy differences between the γ matrix side and the grain boundary side of the γ-γ′ interface provided a driving force for the movement of γ′ phase in this model. In addition, the serrated grain boundary could be described by the serration amplitude and wavelength, which was affected by the solution temperature, soaking time and cooling rate after heat treatment. Grain boundary carbides and borides have also been proved to be the main reason for inducing the formation of serrated grain boundaries [23,24]. The effect of $M_{23}C_6$ carbides on the formation of serrated grain boundaries has been investigated in a wrought Ni-based superalloy [25]. The nucleation and oriented growth of $M_{23}C_6$ carbides at grain boundaries determined the formation of serrated grain boundaries. At the same time, a semi-quantitative model about the grain boundary serration was proposed based on the interfacial energy calculations. The driving force of carbides induced grain boundary serration was related to the different coherence orientation relationship between grain boundary carbides and grains on both sides [26,27]. The coherent phase interface, with lower energy, was relatively stable after carbides nucleation, while the non-coherent phase interface showed higher energy and mobility. Therefore, the carbides were easy to move into the grains on one side, which made the grain boundaries protrude to the incoherent grains, and finally formed a serrated grain boundary. Currently, the formation mechanisms of serrated grain boundary are still inconclusive, and how to optimize heat treatment parameters and distinguish the serrated grain boundaries accurately will be critical.

In the present work, GH4975 superalloy was subjected to heat treatments, including solution treatment and isothermal heat treatment, to investigate the grain boundary serration process. The influences of temperature, soaking time, and cooling rate on the serrated grain boundary morphology were discussed based on the interaction between precipitated phases and grain boundaries, and the serration mechanisms were also explored.

2. Materials and Experimental

The wrought Ni-based superalloy GH4975 was used in this work, which was obtained through vacuum induction-melting, electroslag remelting, and vacuum arc-remelting. The chemical composition (wt.%) of the studied alloy is shown in Table 1. Figure 1 presents the equilibrium phase transformations for GH4975 alloy from 600 to 1400 °C, calculated by using Jmatpro software, and the γ′ solvus temperature was hence estimated to be about 1199 °C. The heat treatments were conducted in a resistance furnace by considering the influences of different treatment parameters on the formation process of serrated grain boundaries. The specific processes of solution treatment and isothermal treatment for the studied alloy were shown in Table 2. Firstly, the samples were treated at 1210 °C for 6 h to ensure that the γ′ phase was dissolved completely. Two cooling conditions, i.e., furnace cooling (FC) and air cooling (AC), were utilized to study the effects of cooling rate on serrated grain boundaries. The cooling rates of AC and FC were determined to be about 250~300 and 4 °C/min, respectively. Then, the isothermal treatments were conducted at 1150, 1160, and 1175 °C with a soaking time of 1 and 2 h.

Table 1. Chemical composition of GH4975 superalloy.

Ni	Co	Cr	Mo	W	Al	Ti	Nb	C	B	Zr
Base	15.5	8.5	1.2	10.0	4.8	2.4	1.5	0.10	0.015	0.04

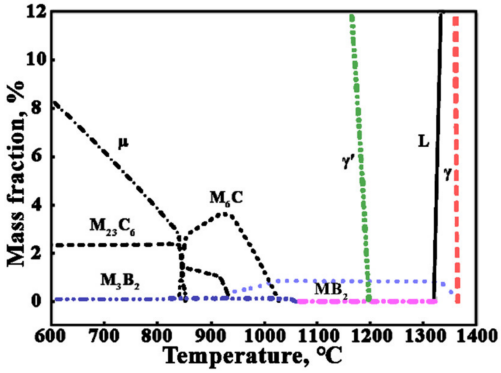

Figure 1. The equilibrium phase diagram of GH4975 alloy obtained by thermodynamic calculation.

Table 2. The processes of solution treatment and isothermal treatment of GH4975 alloy.

No	Solution Treatment	Isothermal Treatment (Temperature, °C)	Isothermal Treatment (Soaking Time, h)
T1	1210 °C × 6 h, AC		
T2	1210 °C × 6 h, FC		
T3	1210 °C × 6 h, FC	1160 °C	1 h
T4	1210 °C × 6 h, FC	1160 °C	2 h
T5	1210 °C × 6 h, FC	1175 °C	2 h
T6	1210 °C × 6 h, FC	1150 °C	2 h

After heat treatments, the samples for optical microscope examination were mechanically polished to obtain mirror surface, and then etched in a solution of 10 mL HCl + 10 mL CH_3CH_2OH + 1 g $CuCl_2$ for 4–10 s at room temperature. The mean equivalent diameter of each grain was measured in order to measure the grain size. The mean grain size (more than 100 grains were measured) was determined by Image-J software. Figure 2 shows the process of the grain size measurement of the studied alloy under isothermally heat treated at the temperature of 1160 °C with the soaking time of 1 h. In addition, the grain boundaries were analyzed to calculate the wavelength and amplitude of serrations, and more than 20 serrations were calculated at each individual condition (Figure 3). For SEM-EBSD analysis, the samples were electropolished in a solution of 20 vol% H_2SO_4 and 80 vol% CH_3OH, and then etched using a solution of 170 mL H_3PO_4 + 10 mL HNO_3 + 15 g CrO_3 at 3–5 V for 4–10 s at room temperature. In addition, the elements' distribution of studied alloy were determined by wavelength dispersive spectrometry (WDS) using an electron probe microanalyzer (EPMA).

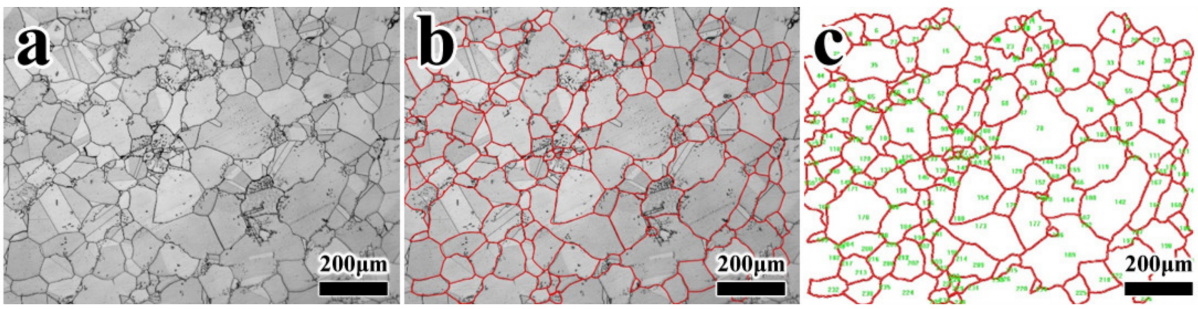

Figure 2. Grain size measurement of GH4975 alloy under isothermally heat treated at the temperature of 1160 °C with a soaking time of 1 h: (**a**) the original image for grain size measurement; (**b**) the digitally processed image; (**c**) grain counting.

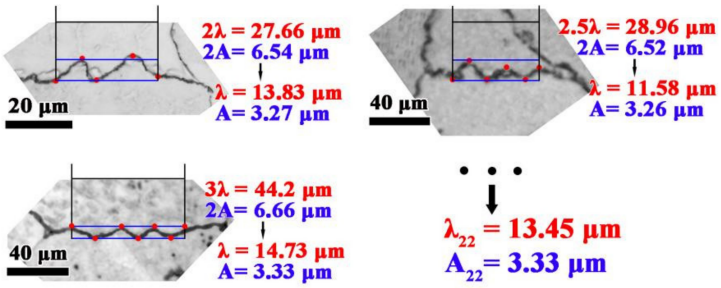

Figure 3. Calculation of the wavelength and amplitude of grain boundary serration.

3. Results and Discussion

3.1. Effect of Heat Treatment on Grain Boundary Morphology

Figure 4 showed the typical microstructure of GH4975 alloy under different heat treatments. Figure 4a,b revealed that the grain size of GH4975 alloy was slightly affected by cooling conditions. The mean grain size was measured to be 94.6 μm when the sample was cooled by air (AC), which was similar to that measured at the cooling condition of FC (92.3 μm). When the studied alloy was isothermally heat treated at the temperature of 1160 °C, the mean grain size increased with the increasing of soaking time, as shown in Figure 5. However, when the studied alloy was heat treated at different temperature, the mean grain size had no obviously change, which indicated that the grain size was more sensitive to soaking time rather than to isothermal heat treatment temperature within the temperature and time ranges utilized in the present work.

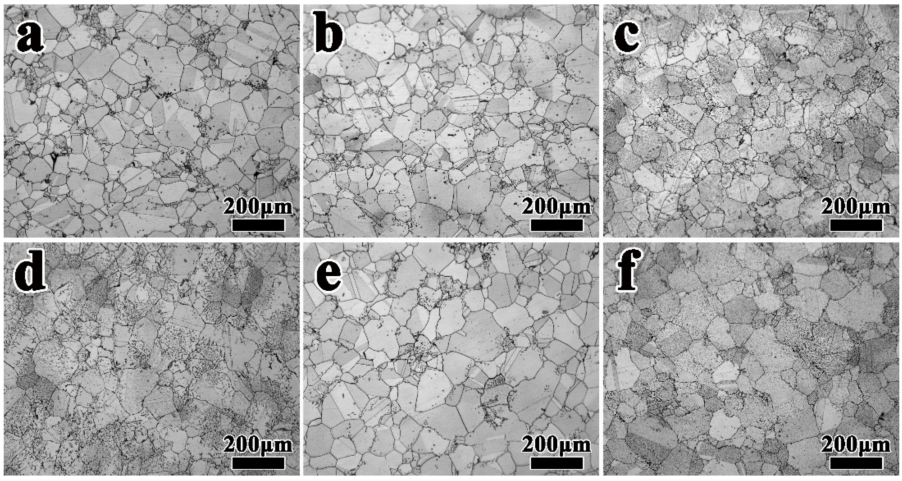

Figure 4. Typical microstructure of GH4975 alloy under different heat treatment conditions: (**a**) T1; (**b**) T2; (**c**) T3; (**d**) T4; (**e**) T5; (**f**) T6.

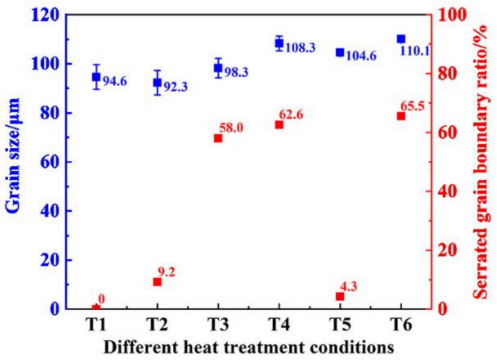

Figure 5. The mean grain size and serrated grain boundary ratio of GH4975 alloy under different heat treatment conditions.

The grain boundary morphology characteristics of the GH4975 samples subjected to different heat treatments are also plotted in Figure 5 by red scatters. By comparison between T1 and T2, it could be confirmed that a slow cooling rate would be appropriate to accelerate the formation of serrated grain boundaries. In the meantime, the results of T2, T3, and T4 also gave a conclusion that the serrated grain boundary ratio increased with the increase of soaking time when the other heat treatment conditions were all constant. It could be observed that the serrated grain boundary ratio was 58.0% and 62.6% at the soaking time of 1 h (T3) and 2 h (T4), respectively. In addition, it should be noted that when the heat treatment temperature increased to 1175 °C (T5), the formation of serrated grain boundary was restrained. The characterization of grain boundary morphology within the samples, subjected to the heat treatments labelled T4, T5, and T6, indicated that the serrated grain boundary ratio decreased with the increase of isothermal heat treatment temperature within the used temperature range. Generally, it could be concluded that the slower cooling rates, the lower isothermally heat treatment temperature, and the longer soaking time could strongly accelerate the formation of serrated grain boundaries within GH4975 superalloy.

Figure 6 showed the typical morphology of serrated grain boundaries under different heat treatment conditions. The serrated grain boundaries were observed under the heat treatment conditions of T3, T4, and T6. It indicated that grain boundary serration occurred after solution treatment with slow cooling condition (FC). In addition, the temperature and soaking time of isothermal treatment also have great effects on the formation of serrated grain boundaries. Both the higher temperature and shorter soaking time did not benefit the formation of serrated grain boundaries. In general, the serrated grain boundaries are defined when the serration amplitude is larger than 0.5 μm, and the wavelength and amplitude of serrated grain boundary is often used to describe the grain boundary morphology. At the isothermal treatment temperature of 1160 °C, the serrated grain boundary wavelength (λ) increased with the soaking time increasing from 1 h to 2 h, while the amplitude (A) decreased with that, as shown in Figure 6c,d. However, when the isothermal treatment temperature decreased from 1160 °C to 1150 °C, the wavelength and amplitude of serrated grain boundaries did not have an obvious change, as shown in Figure 6f. Furthermore, many investigations showed that the formation of serrated grain boundaries were closely related to the precipitated phase. Therefore, further exploration on the interactions between grain boundaries and precipitating phases would be necessary to understand the formation of serrated grain boundaries.

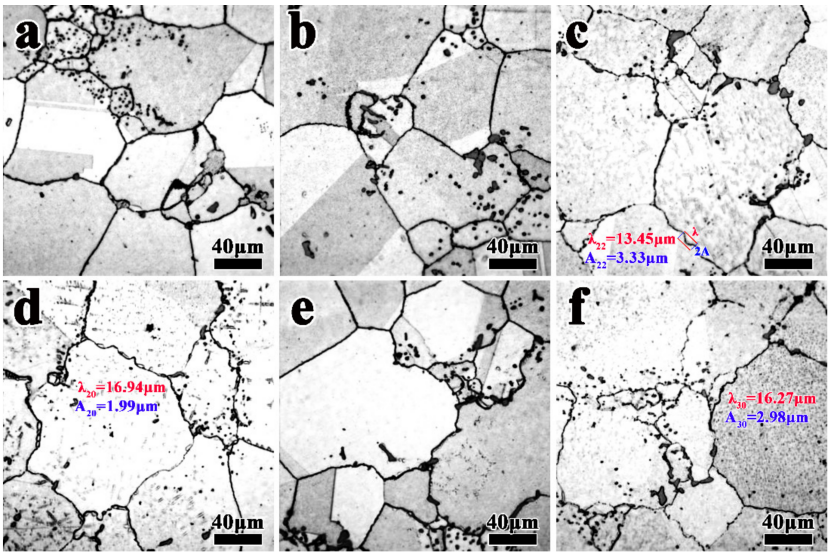

Figure 6. The formation of serrated grain boundaries under different heat treatment conditions: (**a**) T1; (**b**) T2; (**c**) T3; (**d**) T4; (**e**) T5; (**f**) T6.

3.2. Effect of Heat Treatment on Precipitated Phases

It has been well accepted that the formation of serrated grain boundary is strongly influenced by the interactions between grain boundaries and precipitating phases [25–28]. Therefore, a deep assessment about the precipitates, including γ′ phase, MC and $M_{23}C_6$ carbides within GH4975 superalloy, will be necessary for understanding the formation mechanism of the serrated grain boundaries. Figure 7 presented the typical γ′ phase of GH4975 alloy after heat treatment with various cooling conditions, which revealed that the morphology and size of γ′ phase were significantly affected by cooling conditions. When the cooling condition was AC, the cubic γ′ phase formed due to the faster cooling rate, and the mean size was measured to be about 330 nm, as shown in Figure 7a. It was easy to note that the morphology and size of γ′ phase changed significantly with the decrease of the cooling rate. Two types of γ′ phase could be observed under the cooling condition of FC. The cubic γ′ phase with a relatively small size, about 350 nm, was similar to that at AC, as shown in Figure 7b. However, the size of dendritic γ′ phase was relatively larger, and the equivalent diameters ranged from 0.8 to 2 μm, as shown in Figure 7c. The formation of dendritic γ′ phase was related to the slower cooling rate due to the enough time for the diffusion of γ′ phase forming elements. In addition, the lattice mismatch between γ matrix and γ′ phase, and the γ/γ′ interfacial energy, also have great effects on the formation of the dendritic γ′ phase [29–31].

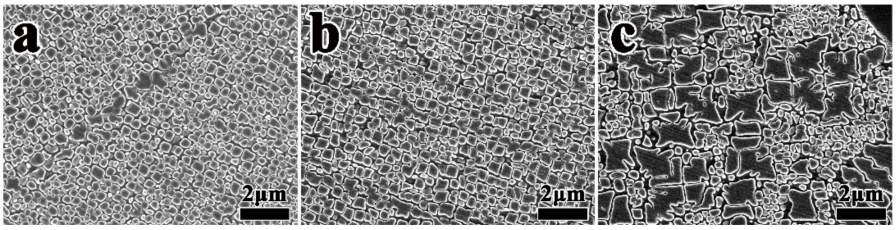

Figure 7. Typical γ′ phase of GH4975 alloy after heat treatment with various cooling conditions: (**a**) AC, cubic γ′ phase; (**b**,**c**) FC, cubic and dendritic γ′ phase, respectively.

Figure 8 showed the morphology and size of γ′ phase under isothermal heat treatment at the temperature of 1160 °C with different soaking time. As shown in Figure 8a, the γ′ phase exhibited a mixture distribution consisting of cubes and dendrites when the soaking time was 0 h, and the dendritic γ′ phase was mostly regular. With the increase of soaking time, the γ′ phase in GH4975 alloy was also composed of cubic and dendritic shapes. However, it should be noted that the content of dendritic γ′ phase decreased and the size of them increased gradually. In addition, a part of γ′ phase were irregular. The long strip γ′ phase (Figure 8b) and cluster γ′ phase (Figure 8c) were formed with the increase of soaking time. It indicates that the soaking time strongly influenced the morphology of γ′ phase, and then would have an impact on the formation of serrated grain boundary. Figure 9 presented the morphology and size distribution of γ′ phase under isothermal heat treatment at different temperatures with the soaking time of 2 h. At the temperature of 1150 °C, the γ′ phase was composed of cubic and dendritic shapes, as shown in Figure 9a. The content of dendritic γ′ phase gradually decreased with the increase of isothermal heat treatment temperature. When the temperature raised up to 1175 °C, the size of cubic γ′ phase was measured to be about 330 nm, as shown in Figure 9c. In summary, the driving force for the formation of γ′ phase is small due to the lower supersaturation of the solid solution at slower cooling condition, which led to the preferentially γ′ phase nucleating at grain boundaries. With the increase of soaking time, the γ′ phase at grain boundaries gradually grew up and then pinned grain boundary to inhibit the migration of grain boundary sections. Although γ′ particles at the grain boundary pinned the grain boundary and then inhibited its migration here, the GB sections far away from the γ′ particles would be able to migrate as normal. The different migration abilities of each GB section leading from pinning effect generated the serrated morphology [32].

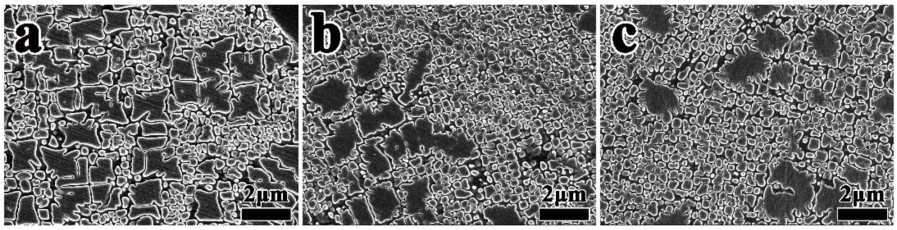

Figure 8. The γ′ phase under isothermal heat treatment at the temperature of 1160 °C with different soaking time: (**a**) 0 h; (**b**) 1 h; (**c**) 2 h.

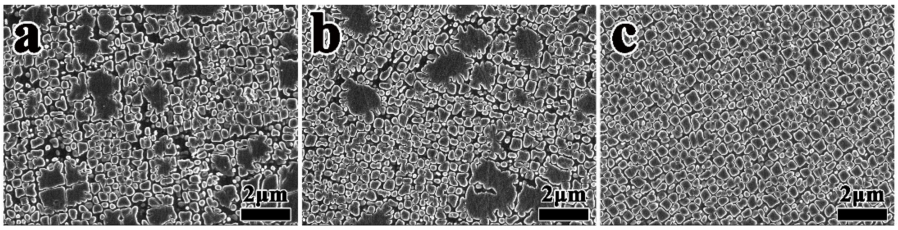

Figure 9. The γ′ phase under isothermal heat treatment at different temperatures with the soaking time of 2 h: (**a**) 1150 °C; (**b**) 1160 °C; (**c**) 1175 °C.

Various carbides and borides precipitated on grain boundaries also deserved a special attention when one focused on the grain boundary morphology [25]. Figure 10 presented the precipitating phase of GH4975 alloy at straight grain boundaries and at serrated grain boundaries, respectively. It could be observed that $M_{23}C_6$ carbides occurred at triangular grain boundaries while mostly M_3B_2 borides existed at straight grain boundaries. The sizes of both precipitating phases were small, which slightly affected the migration of grain boundaries. In addition, there was also a part of larger size MC carbides and M_3C_2 borides at grain boundaries, which impeded the movement of grain boundaries and hence influenced the morphology of grain boundaries. However, it was not enough to promote the formation of serrated grain boundary, as shown in Figure 10a. At the same time, the precipitating phase at serrated grain boundaries after isothermal treatment was obtained. It was observed that a lot of larger size precipitating phases (including γ′ phase, MC carbide and M_3C_2 boride) existed at the grain boundaries. These phases could effectively hinder the migration of grain boundaries during isothermal treatment and then promoted the formation of serrated grain boundaries, as shown in Figure 10b.

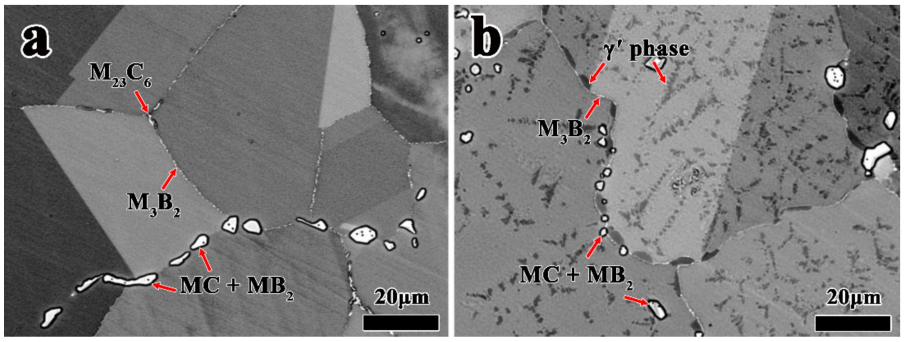

Figure 10. The typical precipitated phase morphology of GH4975 alloy: (**a**) at straight grain boundaries; (**b**) at serrated grain boundaries.

3.3. The Formation Mechanism of Serrated Grain Boundary

Figure 11 showed the microstructure of serrated grain boundaries and γ′ phase within the sample subjected to isothermal treatment. EBSD analysis revealed that the large size γ′ phase existed at the majority of grain boundaries except the twin boundaries, as shown in Figure 11a. It should be noted that the crystal orientations of γ′ phase here was almost

consistent with the grain orientation on one side, but inconsistent with the grain orientation on the other side (Figure 11c). Obviously, the γ′ phase on grain boundaries preferred to grow into the latter one due to the higher migration ability of the incoherent interface between the γ′ phase and the other grain which possessed a distinguish crystal orientation. When the sample was subjected to isothermal treatment, the solute atoms were enriched in γ′ phase. The grain boundary γ′ phase gradually grew up along the direction perpendicular to the grain boundary, which pushed grain boundary section to bulge and finally generated a serrated grain boundary, as shown schematically in Figure 11d.

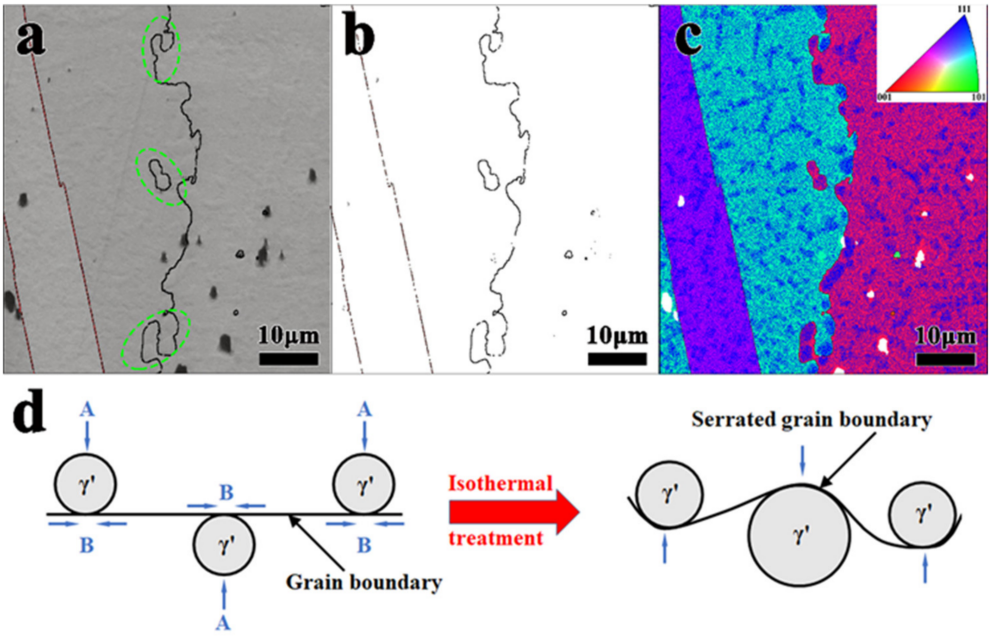

Figure 11. The typical microstructure of the serrated grain boundaries and precipitates after isothermal treatment: (**a**) band contrast map; (**b**) grain boundary maps; (**c**) IPF map; (**d**) schematic map for γ′ phase promoting the formation of serrated grain boundaries.

In addition, grain boundary serration was also related to grain boundary carbides, such as $M_{23}C_6$ and MC carbides [20]. Li et al. investigated the carbide precipitation at grain boundary in Ni-based alloy 690 [33]. The results showed that the boundary carbides were easy to nucleate in the grain with high indexed crystal plane parallel to boundary, and the carbides had coherent orientation relationship (COR) with the grain. The carbides preferentially grew into the grain without COR between carbides and grain, which generated serrated grain boundaries. Figure 12 showed the electron probe micro analyses (EPMA) results of the microstructure containing a serrated grain boundary under isothermal heat treatment with slowly cooling condition (FC). Various precipitates could be detected on the serrated grain boundaries, including borides and γ′ phase. Based on the element distribution map of the selected area, it could be confirmed that the γ′ phase, which re-precipitated in γ matrix (dendritic γ′ phase) or on the serrated grain boundary (long strip shape γ′ phase), was rich in Al, Ti, Ni, and poor in Cr, Co. In addition, some borides and carbides were also observed to precipitate near the serrated grain boundaries, as marked in Figure 11. It indicated that Ti, Nb, C, B, and W preferred to segregate within borides and carbides. In addition, it should be noted that the segregation of γ′-rich elements, as well as the borides or carbides rich elements, also have great effects on the formation of serrated grain boundaries. Furthermore, the slow cooling condition provided enough time for element migration and precipitate growth, which also could promote the formation of serrated grain boundaries.

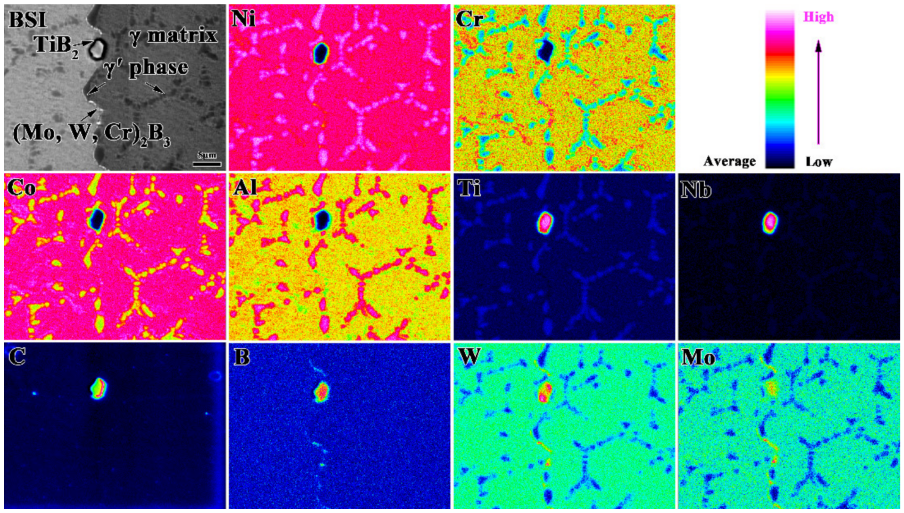

Figure 12. EPMA analyses of the microstructure on serrated grain boundaries under isothermal heat treatment under FC condition.

4. Conclusions

In this work, the solution treatment and isothermal heat treatment with different cooling rates for GH4975 alloy was conducted to investigate the formation process and mechanisms of serrated grain boundaries. The interactions between precipitated phases and grain boundaries were explored in this process. Several conclusions were summarized in the following:

1. The serrated grain boundaries can be obtained by both the solution treatment and isothermal heat treatment, provided that the cooling rates were controlled to be quite slow. Compared with the samples under fast cooling condition (AC), the samples at furnace cooling (FC) condition formed serrated grain boundaries more easily due to a sufficient element diffusion.

2. Isothermal heat treatment temperature and soaking time strongly affected the morphology and size of precipitated phases within GH4975 superalloy, and consequently influenced the formation of serrated grain boundaries.

3. The grain boundary γ' phase gradually grew along the direction perpendicular to the grain boundary, which bent the grain boundary and then formed the serrated grain boundaries. The pinning effects of grain boundary precipitated phase on grain boundary migration also affected the grain boundary morphology strongly.

Author Contributions: Data curation, H.Y.; Formal analysis, B.X.; Funding acquisition, Y.N.; Investigation, S.H. and B.X.; Methodology, S.H., W.Z. and Y.N.; Supervision, B.Z. All authors have read and agreed to the published version of the manuscript.

Funding: This research was funded by China Postdoctoral Science Foundation, grant number 2021M693856l, and Natural Science Foundation of Shaanxi Province of China, grant number 2021JQ-551.

Institutional Review Board Statement: Not applicable.

Informed Consent Statement: Not applicable.

Data Availability Statement: The data presented in this study are available on request from the corresponding author. The data are not publicly available for the time being due to an ongoing study.

Conflicts of Interest: The authors declare no conflict of interest.

References

1. Nicolaÿ, A.; Fiorucci, G.; Franchet, J.M.; Cormier, J.; Bozzolo, N. Influence of strain rate on subsolvus dynamic and post-dynamic recrystallization kinetics of Inconel 718. *Acta Mater.* **2019**, *174*, 406–417. [CrossRef]
2. Ning, Y.Q.; Yao, Z.K.; Lei, Y.Y.; Guo, H.Z.; Fu, M.W. Hot deformation behavior of the post-cogging FGH4096 superalloy with fine equiaxed microstructure. *Mater. Charact.* **2011**, *62*, 887–893. [CrossRef]
3. Lawitzki, R.; Hassan, S.; Karge, L.; Wagner, J.; Wang, D.; von Kobylinski, J.; Krempaszky, C.; Hofmann, M.; Gilles, R.; Schmitz, G. Differentiation of γ'- and γ''- precipitates in Inconel 718 by a complementary study with small-angle neutron scattering and analytical microscopy. *Acta Mater.* **2019**, *163*, 28–39. [CrossRef]
4. Xie, B.C.; Yu, H.; Sheng, T.; Xiong, Y.H.; Ning, Y.Q.; Fu, M.W. DDRX and CDRX of an as-cast nickel-based superalloy during hot compression at γ' sub-/super-solvus temperatures. *J. Alloys Compd.* **2019**, *803*, 16–29. [CrossRef]
5. Zhang, B.Y.; Wang, Z.T.; Yu, H.; Ning, Y.Q. Microstructural origin and control mechanism of the mixed grain structure in Ni-based superalloys. *J. Alloys Compd.* **2022**, *900*, 163515. [CrossRef]
6. Tanaka, M.; Iizuka, H.; Ashihara, F. Effects of serrated grain boundaries on the crack growth in austenitic heat-resisting steels during high-temperature creep. *J. Mater. Sci.* **1988**, *23*, 3827–3832. [CrossRef]
7. Tanaka, M.; Miyagawa, O.; Sakaki, T.; Iizuka, H.; Ashihara, F.; Fujishiro, D. Creep rupture strength and grain-boundary sliding in austenitic 21 Cr-4Ni-9Mn steels with serrated grain boundaries. *J. Mater. Sci.* **1988**, *23*, 621–628. [CrossRef]
8. Hong, H.U.; Nam, S.W. The occurrence of grain boundary serration and its effect on the $M_{23}C_6$ carbide characteristics in an AISI 316 stainless steel. *Mater. Sci. Eng. A* **2002**, *332*, 255–261. [CrossRef]
9. Bhuyan, P.; Reddy, K.V.; Pradhan, S.K.; Pal, S.; Mitra, R.; Mandal, S. A potential insight into the serration behaviour of $\Sigma 3^n$ ($n \leq 3$) boundaries in Alloy 617. *Mater. Chem. Phys.* **2020**, *248*, 122919. [CrossRef]
10. Tang, Y.T.; Karamched, P.; Liu, J.; Haley, J.C.; Reed, R.C.; Wilkinson, A.J. Grain boundary serration in nickel alloy inconel 600: Quantification and mechanisms. *Acta Mater.* **2019**, *181*, 352–366. [CrossRef]
11. Jeong, C.Y.; Kim, K.J.; Hong, H.U.; Nam, S.W. Effects of aging temperature and grain size on the formation of serrated grain boundaries in an AISI 316 stainless steel. *Mater. Chem. Phys.* **2013**, *139*, 27–33. [CrossRef]
12. Kim, K.J.; Hong, H.U.; Nam, S.W. A study on the mechanism of serrated grain boundary formation in an austenitic stainless steel. *Mater. Chem. Phys.* **2011**, *126*, 480–483. [CrossRef]
13. Hong, H.U.; Kim, I.S.; Choi, B.G.; Kim, M.Y.; Jo, C.Y. The effect of grain boundary serration on creep resistance in a wrought nickel-based superalloy. *Mater. Sci. Eng. A* **2009**, *517*, 125–131. [CrossRef]
14. Li, H.Y.; Sun, J.F.; Hardy, M.C.; Evans, H.E.; Williams, S.J.; Doel, T.J.A.; Bowen, P. Effects of microstructure on high temperature dwell fatigue crack growth in a coarse grain PM nickel based superalloy. *Acta Mater.* **2015**, *90*, 355–369. [CrossRef]
15. Tang, Y.T.; Wilkinson, A.J.; Reed, R.C. Grain boundary serration in nickel-based superalloy Inconel 600: Generation and effects on mechanical behavior. *Metall. Mater. Trans. A* **2018**, *49*, 4324–4342. [CrossRef]
16. Koul, A.K.; Gessinger, G.H. On the mechanism of serrated grain boundary formation in Ni-based superalloys. *Acta Mater.* **1983**, *31*, 1061–1069. [CrossRef]
17. Atrazhev, V.V.; Burlatsky, S.F.; Dmitriev, D.V.; Furrer, D.; Kuzminyh, N.Y.; Lomaev, I.L.; Novikov, D.L.; Stolz, S.; Reynolds, P. The mechanism of grain boundary serration and fan-type structure formation in Ni-based superalloys. *Metall. Mater. Trans. A* **2020**, *51*, 3648–3657.
18. Lu, X.D.; Deng, Q.; Du, J.H.; Qu, J.L.; Zhuang, J.Y.; Zhong, Z.Y. Effect of slow cooling treatment on microstructure of difficult deformation GH4742 superalloy. *J. Alloys Compd.* **2009**, *477*, 100–103. [CrossRef]
19. Mitchell, R.J.; Li, H.Y.; Huang, Z.W. On the formation of serrated grain boundaries and fan type structures in an advanced polycrystalline nickel-base superalloy. *J. Mater. Process. Technol.* **2009**, *209*, 1011–1017. [CrossRef]
20. Lim, Y.S.; Kim, D.J.; Hwang, S.S.; Kim, H.P.; Kim, S.W. $M_{23}C_6$ precipitation behavior and grain boundary serration in Ni-based Alloy 690. *Mater. Charact.* **2014**, *96*, 28–39. [CrossRef]
21. Lu, X.D.; Du, J.H.; Deng, Q.; Zhong, Z.Y. Effect of slow cooling treatment on hot deformation behavior of GH4742 superalloy. *J. Alloys Compd.* **2009**, *486*, 195–198. [CrossRef]
22. Yang, K.; An, T.; Qu, J.L.; Du, J.H.; Qin, H.L.; Zheng, S.Q.; Bi, Z.N. Effects of solution cooling rate on the grain boundary and mechanical properties of GH4710 alloy. *Mater. Sci. Eng. A* **2022**, *832*, 142459. [CrossRef]
23. Hong, H.U.; Jeong, H.W.; Kim, I.S.; Choi, B.G.; Yoo, Y.S.; Jo, C.Y. A study on the formation of serrated grain boundaries and its applications in Nimonic 263. *Mater. Sci. Forum.* **2010**, *638–642*, 2245–2250. [CrossRef]
24. Kim, K.J.; Hong, H.U.; Nam, S.W. Investigation on the formation of serrated grain boundaries with grain boundary characteristics in an AISI 316 stainless steel. *J. Nucl. Mater.* **2009**, *393*, 249–253. [CrossRef]
25. Jiang, L.; Hu, R.; Kou, H.C.; Li, J.S.; Bai, G.H.; Fu, H.Z. The effect of $M_{23}C_6$ carbides on the formation of grain boundary serrations in a wrought Ni-based superalloy. *Mater. Sci. Eng. A* **2012**, *536*, 37–44. [CrossRef]
26. Zhao, X.; Wang, M.; Hao, X.C.; Zha, X.D.; Gao, M.; Ma, Y.C.; Liu, K. Research progress in grain boundary serration in iron/nickel based austenitic polycrystalline alloys. *Chin. J. Eng.* **2021**, *43*, 1323–1338.
27. Haack, M.; Kuczyk, M.; Seidel, A.; López, E.; Brückner, F.; Leyens, C. Investigation on the formation of grain boundary serrations in additively manufactured superalloy Haynes 230. *J. Laser Appl.* **2020**, *32*, 032014. [CrossRef]
28. Son, H.W.; Lee, J.W.; Hyun, S.K. Mechanism of grain boundary serration during hot deformation of AZ31 alloy: Role of grain boundary dislocations and grain boundary sliding. *Int. J. Plasticity* **2020**, *125*, 118–132. [CrossRef]

29. Zhang, Y.J.; Huang, Y.J.; Yang, L.; Li, J.G. Evolution of microstructures at a wide range of solidification cooling rate in a Ni-based superalloy. *J. Alloys Compd.* **2013**, *570*, 70–75. [CrossRef]
30. Fan, X.Q.; Guo, Z.P.; Wang, X.F.; Yang, J.; Zou, J.W. Morphology evolution of gamma' precipitates in a powder metallurgy Ni-base superalloy. *Mater. Charact.* **2018**, *139*, 382–389. [CrossRef]
31. Yu, H.; Wang, Z.T.; Zhang, B.Y.; Ning, Y.Q.; Fu, M.W. Re-precipitation mechanisms of the γ' phase with sphere, near-sphere, cubic, octets and finally-dendrite in as-cast Ni-based superalloys. *J. Alloys Compd.* **2021**, *876*, 160104. [CrossRef]
32. Mao, W.M.; Yang, P. Migration behaviors of boundaries in polycrystalline metals during grain growth process. *Sci. Sin. Technol.* **2014**, *44*, 911–916.
33. Li, H.; Xia, S.; Zhou, B.X.; Peng, J.C. Study of carbide precipitation at grain bundary in nickel base alloy 690. *Acta Metall. Sin.* **2011**, *47*, 853–858.